ACS SENSORS

pubs.acs.org/acssensors

Article

tdLanYFP, a Yellow, Bright, Photostable, and pH-Insensitive Fluorescent Protein for Live-Cell Imaging and Förster Resonance Energy Transfer-Based Sensing Strategies

Yasmina Bousmah, Hana Valenta, Giulia Bertolin, Utkarsh Singh, Valérie Nicolas, Hélène Pasquier, Marc Tramier, Fabienne Merola, and Marie Erard*

Cite This: *ACS Sens.* 2021, 6, 3940–3947

Read Online

ACCESS | Metrics & More | Article Recommendations | Supporting Information

ABSTRACT: Yellow fluorescent proteins (YFPs) are widely used as optical reporters in Förster resonance energy transfer (FRET)-based biosensors. Although great improvements have been done, the sensitivity of the biosensors is still limited by the low photostability and the poor fluorescence performances of YFPs at acidic pH values. Here, we characterize the yellow fluorescent protein tdLanYFP, derived from the tetrameric protein from the cephalochordate *Branchiostoma lanceolatum*, LanYFP. With a quantum yield of 0.92 and an extinction coefficient of 133,000 $mol^{-1} \cdot L \cdot cm^{-1}$, it is, to our knowledge, the brightest dimeric fluorescent protein available. Contrasting with EYFP and its derivatives, tdLanYFP has a very high photostability *in vitro* and in live cells. As a consequence, tdLanYFP allows imaging of cellular structures with subdiffraction resolution using STED nanoscopy and is compatible with the use of spectromicroscopies in single-molecule regimes. Its very low $pK_{1/2}$ of 3.9 makes tdLanYFP an excellent tag even at acidic pH values. Finally, we show that tdLanYFP is a valuable FRET partner either as a donor or acceptor in different biosensing modalities. Altogether, these assets make tdLanYFP a very attractive yellow fluorescent protein for long-term or single-molecule live-cell imaging including FRET experiments at acidic pH.

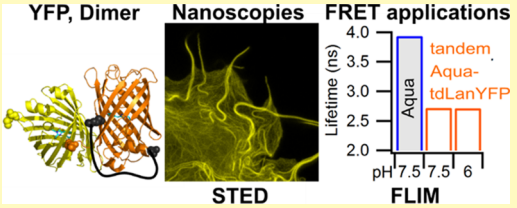

KEYWORDS: *fluorescence imaging, yellow fluorescent protein, genetically encoded biosensor, photobleaching, STED, FRET/FLIM*

Fluorescent proteins (FPs) are used as optical reporters in various biosensing modalities to explore cellular chemistry or cell signaling pathways *in situ*. In particular, FPs are often used in experiments, taking advantage of the Förster resonance energy transfer (FRET) phenomenon.[1] For FRET, a pair of donor/acceptor FPs is required, with the fluorescence spectrum of the donor overlapping the absorption spectrum of the acceptor.[2] If the donor and acceptor are fused to two proteins of interest, FRET can be used to probe protein−protein interactions.[3] It is also possible to fuse them on both sides of a sensing module to build the so-called FRET intramolecular biosensors, which are useful tools to monitor variations in ion or metabolite concentrations[1] or to follow enzymatic activities[4] in living cells. The sensitivity and reliability of FRET-based biosensors depend on the specifications of the donor/acceptor pair such as a simple photophysical behavior with mono-exponential fluorescence decay and limited excited-state reactions, efficient maturation, and high molecular brightness.

In most FRET experiments (~60%), a cyan FP is chosen as the donor and a yellow one as the acceptor.[5,6] For CFPs, variants with low sensitivity to their environment, efficient maturation, high brightness including quantum yield close to 1, and good photostability are now available (Aquamarine,[7] mTurquoise,[8] and mTurquoise2[9]). The best ones notably display a low $pK_{1/2}$, the pH value, at which 50% of the fluorescence intensity is lost, down to 3.1, which is compatible with detection of biological events in acidic environment.[5] This feature opens opportunities to develop FRET-based biosensors dedicated to the real-time visualization of metabolic activities in acidic environments, whether it is due to local pH variations or due to their localization in intracellular compartments.[10−12]

Concerning the acceptor, EYFP served as a template for several rounds of engineering, leading to improved versions of YFPs as mCitrine[13,14] or mVenus[15] and Citrine2.[16] Citrine is less sensitive to chloride ions and pH than EYFP but displays poor photostability.[13] The improvement of the photostability of mCitrine leads to Citrine2, which additionally retained high brightness.[16] Despite these efforts, none of the YFPs derived from EYFP are compatible with the monitoring of biochemical processes in an acidic environment so far, with their $pK_{1/2}$ ranging from 5.3 to 6.[16−18] Consequently, no FRET biosensors based on a cyan/yellow pair were developed for measurements at low pH values.[19]

Received: April 27, 2021
Accepted: October 5, 2021
Published: October 22, 2021

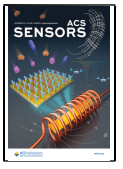

https://doi.org/10.1021/acssensors.1c00874
ACS Sens. 2021, 6, 3940–3947

Table 1. *In Vitro* Characterization of YFPs

	dLanYFP	EYFP	Venus (EYFP F46L-F64L-M153T-V163A-S175G)	Citrine (EYFP Q69M)
λ_{max} excitation (nm)	512	514	515	515
λ_{max} emision (nm)	519	527	528	527
extinction coefficient per chromophore ($mol^{-1}\cdot L\cdot cm^{-1}$)	133,000 ± 8000[a]	84,000 ± 5000	107,000 ± 6400	91,000 ± 5500
quantum yield	0.92 ± 0.05	0.79 ± 0.05	0.78 ± 0.05	0.83 ± 0.05
rel. brightness per chromophore	1.84	1	1.27	1.08
ave. fluo. lifetime[a] (± 0.1 ns)	2.9[b]	3.2	2.9	3.3
$pK_{1/2}$ (± 0.1), $[Cl^-]$ = 85 mM[c]	3.9	6.6	5.9	5.7
chloride affinity, K_{app} (mM)[d]	135 ± 40	70 ± 20	>250	>300
photobleaching decay time (s) on agarose beads[e]	687 ± 15	102 ± 20	49 ± 10	37 ± 10
photobleaching decay time (s) live cells[e]	463 ± 15	44 ± 5	ND	22 ± 5

[a]Exc. 515 nm, em. 580 nm, 20 °C, pH 8. [b]Neg. exponent 0.19 ns, 3%@em. 535 nm, <0.5%@em. 580 nm. [c]Values obtained with the processing of the absorption spectra. [d]Affinities are the average of the values derived from the fits of the data obtained from the processing of the absorption and fluorescence spectra. [e]Under constant wide-field illumination: ex. 500 nm, em. 542 nm, 0.4 W/cm^2.

LanYFP, a yellow tetrameric FP from *Branchiostoma lanceolatum*, has been intensively engineered by Shaner *et al.*, leading to the blue-shifted monomeric variant mNeonGreen.[17,20] While LanYFP has a low $pK_{1/2}$ of 3.5,[17] the pH sensitivity of mNeonGreen is equivalent to that of mCitrine ($pK_{1/2,mNeonGreen} \approx 5.4–5.7$).[17,18] Yet, mNeonGreen has better photostability than mCitrine under the same irradiation conditions.[17,18] mNeonGreen's brightness is also slightly better (~1.5 times) than all available yellow variants.[17,18] Following these observations, we became interested in the intermediate dimeric version, dLanYFP, obtained along the genetic engineering of mNeonGreen. Here, we present a complete characterization of dLanYFP *in vitro* and evaluate the potential given by its tandem version, tdLanYFP, for live-cell imaging. Especially, we highlight its performance as a FRET partner in genetically encoded biosensors even at acidic pH and its suitability for super-resolution microscopy thanks to its very high photostability.

RESULTS AND DISCUSSION

Biochemical Parameters and Fluorescence Characterization of dLanYFP. dLanYFP was produced as a recombinant protein in *Escherichia coli*. Although it is expressed as a monomer, a strong spontaneous dimer formation was observed with size exclusion chromatography and on SDS-PAGE where these dimers dissociated only after heating the sample (Figure S1). We compared the spectroscopic properties of purified dLanYFP to those of the widely used EYFP, Citrine, and Venus. All absorption and fluorescence spectra are equivalent, with a slight blue shift of the absorption and emission maxima of dLanYFP's spectra by 3 and 8 nm, respectively (Figure S2 and Table 1). Therefore, dLanYFP can directly replace standard YFPs without adaptation of spectral selections. Its molar extinction coefficient, evaluated per chromophore with the BCA assay, is 133,000 $mol^{-1}\cdot L\cdot cm^{-1}$ and its quantum yield is 0.92 (Table 1). Those values are consistent with the ones reported by Shaner *et al.*[17] The relative brightness of the fluorophore in dLanYFP is thus improved by nearly a factor of two compared to EYFP, which is remarkable considering that their chromophores are identical (Gly-Tyr-Gly). dLanYFP, together with its parent LanYFP, thus ranges among the brightest fluorescent proteins known today. In live cells, the strong dimer formation by dLanYFP will double the quantity of labeling fluorophores, leading to a potential 4-fold gain in brightness for fluorescence imaging, as compared to the tagging with conventional YFPs. The fluorescence decays of the purified proteins were acquired using the time-correlated single-photon counting (TCSPC) technique upon excitation at 515 nm (Figure S3 and Table 1). For Venus, Citrine, and EYFP, the decays are well fitted by near-single exponentials (>92–94% of the amplitude), with lifetimes in the range of 3 ns, consistent with the literature.[21] The decay of dLanYFP is also mostly mono-exponential (>97%), with a lifetime in a similar range (2.9 ± 0.1 ns). Interestingly, it also includes a small contribution of a negative, very short component, not present in other YFPs, whose proportion depends on the emission wavelength, suggesting some fast reaction in the excited state (Figure S3).

The irreversible photobleaching rate of dLanYFP was compared with the ones of other YFPs immobilized on agarose beads (Figure S4 and Table 1). Under constant illumination into their major absorption band performed with a wide-field microscope, the fluorescence intensity decrease was slower (15–20 times) for dLanYFP in comparison to the other YFPs. This makes this YFP attractive for imaging applications under intense or prolonged illumination.

The YFP's chromophore contains a phenol moiety that exists both in protonated and deprotonated forms, the latter one being fluorescent. It has been shown that $pK_{1/2}$ depends on the chloride ion concentration, which can undergo large variations in biological systems. We compared the $pK_{1/2}$ of dLanYFP with the ones of the YFPs for different chloride ion concentrations in the medium (Figures S5 and S6 and Table 1). Consistent with the literature, the $pK_{1/2}$ of EYFP depends strongly on it and is higher than the ones of Citrine and Venus.[13,17,19] For dLanYFP, the $pK_{1/2}$ also depends on the chloride ion concentration but is significantly lower regardless of its value in comparison to Citrine, leading to a $pK_{1/2}$ of 3.9 ± 0.1 at $[Cl^-]$ = 85 mM. It is an unprecedented value for a YFP that is consistent with the low $pK_{1/2}$ of 3.5 of its parent, LanYFP.[17]

Finally, we also evaluated the maturation kinetics of dLanYFP that was slower than the one of Citrine (Figure S7; rise times of 8300 ± 300 and 3100 ± 100 s for dLanYFP and Citrine, respectively) while remaining in the same order of magnitude or faster than the best CFPs used as a donor in combination with YFPs.[7] It is likely that the dimeric character of dLanYFP slowed down the maturation rate compared to the monomeric mNeonGreen.[21] Such a phenomenon was also

https://doi.org/10.1021/acssensors.1c00874
ACS Sens. 2021, 6, 3940–3947

reported for DsRed and its dimeric and monomeric derivatives.[22]

The Tandem Version tdLanYFP: From Expression in Live Cells to Applications in Spectromicroscopy. The dimerization tendency of dLanYFP might have deleterious consequences in live-cell imaging by forcing nonphysiological intermolecular interactions of its fusion constructs. To remove this drawback, we promoted the formation of a stable intramolecular dimer of dLanYFP by concatenating two copies of the gene separated by a sequence coding for a 19-amino-acid linker (Figure S8) as it was previously done with other existing FP dimers such as dTomato.[22,23] We verified that the spectroscopic properties of tdLanYFP *in vitro* were similar to the ones of dLanYFP (Figure S2). To evaluate the tendency of tdLanYFP to oligomerize, the organized smooth endoplasmic reticulum (OSER) assay was performed in comparison with mCitrine (Citrine A206K).[24] The percentage of COS7 cells transfected with CytERM-tdLanYFP presenting whorled structures of the endoplasmic reticulum triggered by FP oligomerization was evaluated, and typical examples of OSER-positive cases for both proteins are shown in Figure S9. For mCitrine, our evaluation of 95% non-OSER situations is consistent with the literature.[18] For the tandem version, the score of 62% non-OSER cases is in the same range as for tdTomato (57%) and overcomes Citrine (36%).[18] We also observed the appropriate localization of tdLanYFP expressed alone in live cells (Figure 1A) or in fusion with signal peptides targeting the protein to the plasma membrane (Figure 1B) or the cytoskeleton (Figure 1C). In addition, we also fused tdLanYFP to the C-terminus of $p67^{phox}$, a cytosolic protein of the NADPH oxidase complex that is responsible for the superoxide anion production in many cell types.[25] A representative fluorescence lifetime image (FLIM) of COS7 cells expressing p67-tdLanYFP and the corresponding fluorescence decay are presented in Figure 1D,E. The average fluorescence lifetime of tdLanYFP fused to $p67^{phox}$ is similar to that of the purified protein recorded *in vitro* (less than 3% of variation), showing little influence of the concatenation of the momoners and of the fusion on this photophysical parameter.

The photostability of tdLanYFP was confirmed in live cells, along wide-field and confocal imaging, in comparison to Citrine and EYFP (Figure S10). Under wide-field illumination, the characteristic time constants recorded in the cell cytosol were close to the one obtained *in vitro* (Table 1). In confocal imaging, FPs were fused to the actin-targeting sequence, LifeAct, to avoid any diffusion between the recordings of two successive frames. Again, tdLanYFP was more photostable than mCitrine and bleached two to three times slower (Figure S10B). The rates of irreversible photobleaching are known to highly depend on the excitation regimes and it is not surprising to observe a difference between (i) homogeneous and continuous wide-field excitation and (ii) the more intense confocal regime where a laser is transiently focused on a single pixel.

Owing to this high photostability, we evaluated the performance of tdLanYFP for stimulated emission depletion (STED) nanomicroscopy using COS7 transiently expressing LifeAct-tdLanYFP (Figure 2). Due to cell movements between two frames, tracking and quantification of the fluorescence intensities of one single filament were subjected to some variability. Nevertheless, we estimated that only 30% of fluorescence was lost after 40 frames. This result gives

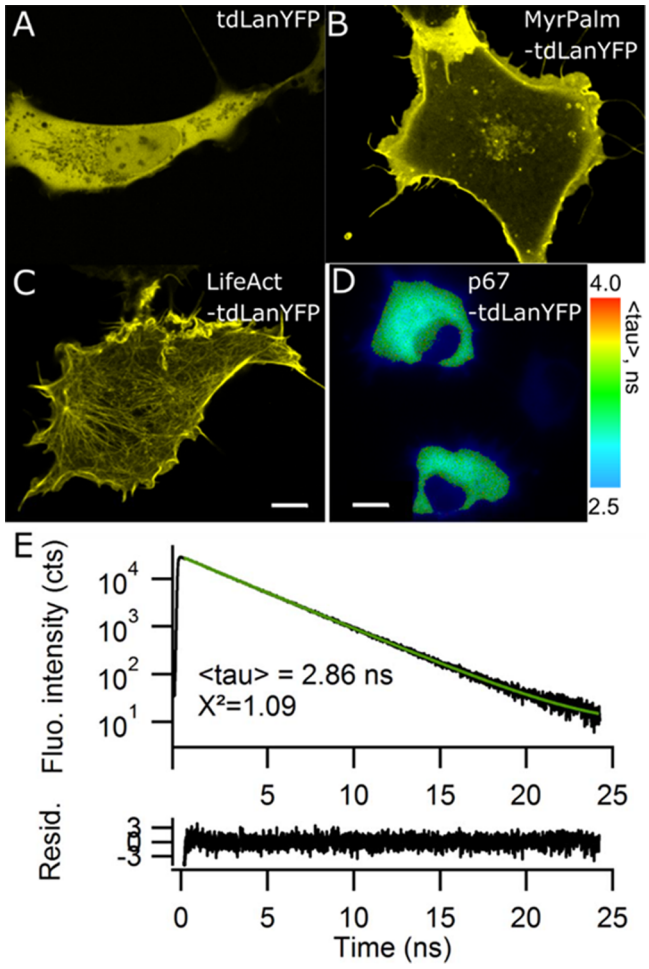

Figure 1. Fluorescence imaging and TCSPC fluorescence decays of tdLanYFP in COS7 cells. Confocal microscopy images of tdLanYFP targeted to (A) the cytosol, (B) membrane, and (C) cytoskeleton. Scale bar, 10 μm. (D) Intensity (gray scale) and fluorescence lifetime (color scale) image of a fusion p67-tdLanYFP. Scale bar, 15 μm. (E) Fluorescence photons collected from the upper cell were used to calculate the corresponding fluorescence decay. The decay was best fitted with a biexponential fit function (green). The residuals of the fit are displayed below the decay.

opportunities for kinetic analysis and organelle tracking with tdLanYFP using STED microscopy.

The combination of high brightness with strong photostability is particularly attractive for experiments in single-molecule regimes such as for fluorescence correlation spectroscopy (FCS), which monitors the diffusion of a few fluorescent molecules in and out of a confocal volume. In the representative example shown in Figure 3, the fluctuations of the fluorescence intensity of cytosolic tdLanYFP were stable over 60 s, and the amplitude of the autocorrelation function ($1/N$) of those fluctuations corresponded to $N = 4$ fluorophores. This possibility to monitor the fluorescence of only a few molecules is the consequence of the high photostability of tdLanYFP, but it is also due to its improved brightness in comparison to the other YFPs for which there are, indeed, only a few examples of live-cell FCS experiments despite their widespread use in live-cell fluorescence imaging.

Characterization of a Model FRET System: Aquamarine-tdLanYFP FRET Fusion. The theoretical Förster distances R_0, at which the donor/acceptor FRET efficiency is

https://doi.org/10.1021/acssensors.1c00874
ACS Sens. 2021, 6, 3940−3947

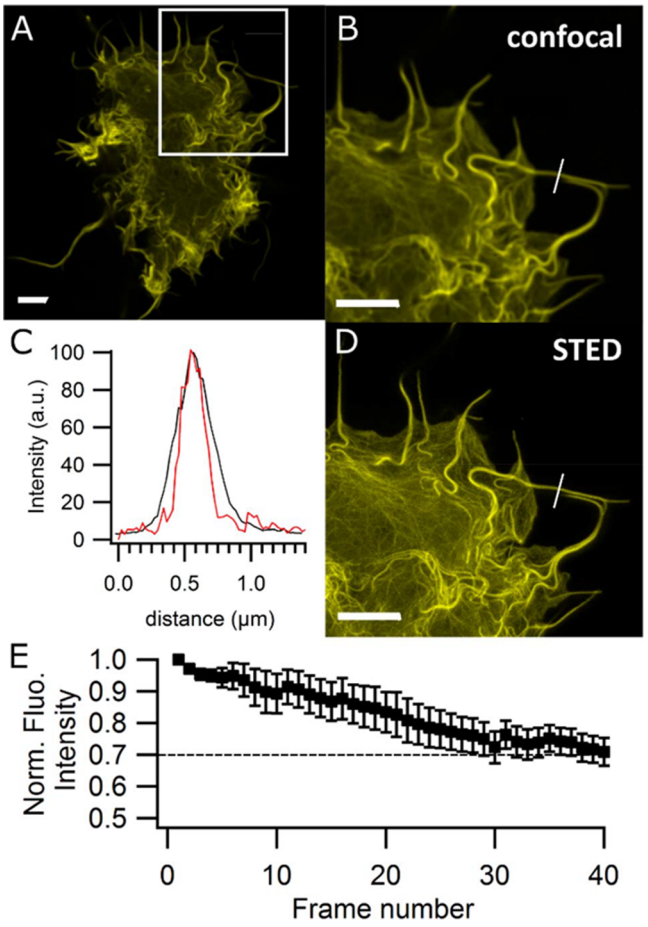

Figure 2. (A) Confocal image of a whole COS7 cell expressing LifeAct-tdLanYFP and (B, D) confocal and STED images of the white ROI. (C) Graph of the plot profile along the white line to show the gain in resolution. (E) Average of the fluorescence intensity decay in 5 ROIs along the actin filaments of the cell during a 40-frame time lapse. Scale bars, 5 μm.

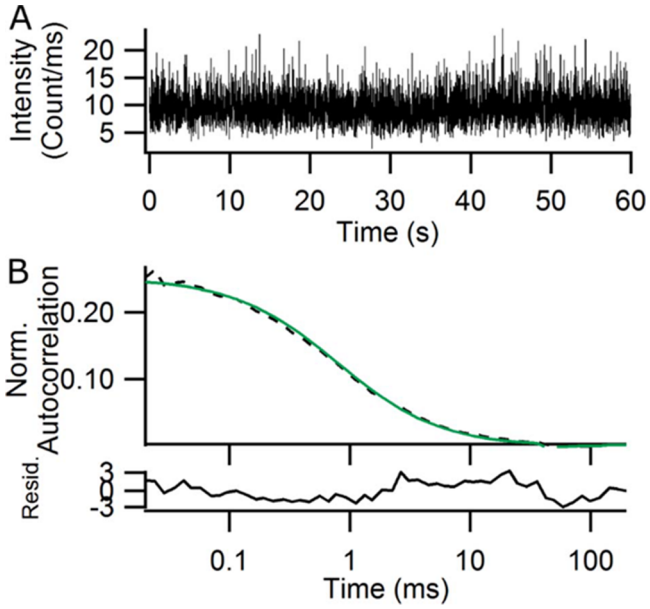

Figure 3. (A) Fluctuations of fluorescence intensity and (B) the corresponding autocorrelation curve acquired in the cytosol of one representative COS7 cell expressing cytosolic tdLanYFP. Experimental values are represented as the dashed line, and their fit is in green. The residuals of the fit are displayed below the autocorrelation curve.

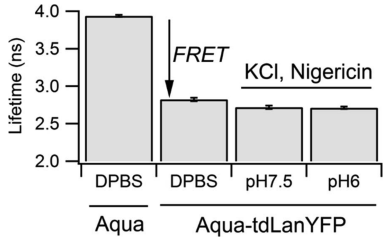

Figure 4. Fluorescence lifetimes of Aquamarine expressed in the cell cytosol of COS7 alone or in tandem with tdLanYFP at different pH values. Average of minimum 20 cells. Values displayed ±SE.

50%, were calculated as 60.4 and 67.8 Å for the FRET pair Aquamarine/dLanYFP as a monomer or dimer, respectively (κ^2 = 2/3, n = 1.33). It is slighty above another CFP/YFP FRET pair (50−60 Å, www.fpbase.org[26]). To evaluate the performance of tdLanYFP as an acceptor in FRET-based imaging applications, we built a FRET fusion Aquamarine-tdLanYFP and compared its response monitored by FLIM in COS7 cells to the previously studied Aquamarine-Citrine fusion (Figure 4).[19] We also recorded the overall fluorescence spectra upon donor excitation in a field of view under the microscope (Figure S11). The average lifetime of Aquamarine in the Aquamarine-tdLanYFP FRET fusion is significantly lower than the one of Aquamarine expressed alone (2.80 ± 0.11 and 3.95 ± 0.08 ns, respectively), showing a strong energy transfer from Aquamarine to tdLanYFP, giving an average FRET efficiency of 28% (Figure 4). This FRET is also clearly observed in the fluorescence spectrum through the presence of an intense fluorescence band between 520 and 530 nm, characteristic of the acceptor fluorescence emission triggered by donor excitation and energy transfer (Figure S11). The calculated FRET efficiency is similar to the one observed in the original Aquamarine-Citrine construct (32%). This is surprising, considering that in the new construct, each Aquamarine donor is linked to two dLanYFP moieties, each with an increased extinction coefficient in comparison to Citrine. This might arise from the unfavorable relative orientation and/or distance of donor and acceptor chromophores in this particular FRET fusion. Alternatively, it might reflect the occurrence of dark, non-absorbing dLanYFP molecules, for example, due to incomplete chromophore maturation.

To evaluate the effect of pH on the FRET efficiency in the construct Aquamarine-tdLanYFP, the intracellular pH was fixed at either pH 7.5 or pH 6 using a mixture of MES (15 mM) and HEPES (15 mM) buffers containing 140 mM KCl and 10 μM nigericin. Within this pH range, Aquamarine's lifetime did not vary,[7] and indeed, we observed the same lifetime for FRET fusion at both pH values (Figure 4, 2.72 ± 0.11 and 2.72 ± 0.0.9 ns at pH 7.5 and pH 6, respectively). This is an improvement compared to the Aquamarine/Citrine pair whose FRET efficiency changes in function of pH below pH 7.[19] Indeed, acidic pH values induce the formation of the protonated form of Citrine whose absorption band, appearing at lower wavelenghts than the deprotonated form, leads to a poor spectral overlay with the donor fluorescence emission spectrum.[19] As a consequence, the FRET pair Aquamarine/tdLanYFP is thus suitable for FRET studies at acidic pH values at least down to pH 6.

https://doi.org/10.1021/acssensors.1c00874
ACS Sens. 2021, 6, 3940−3947

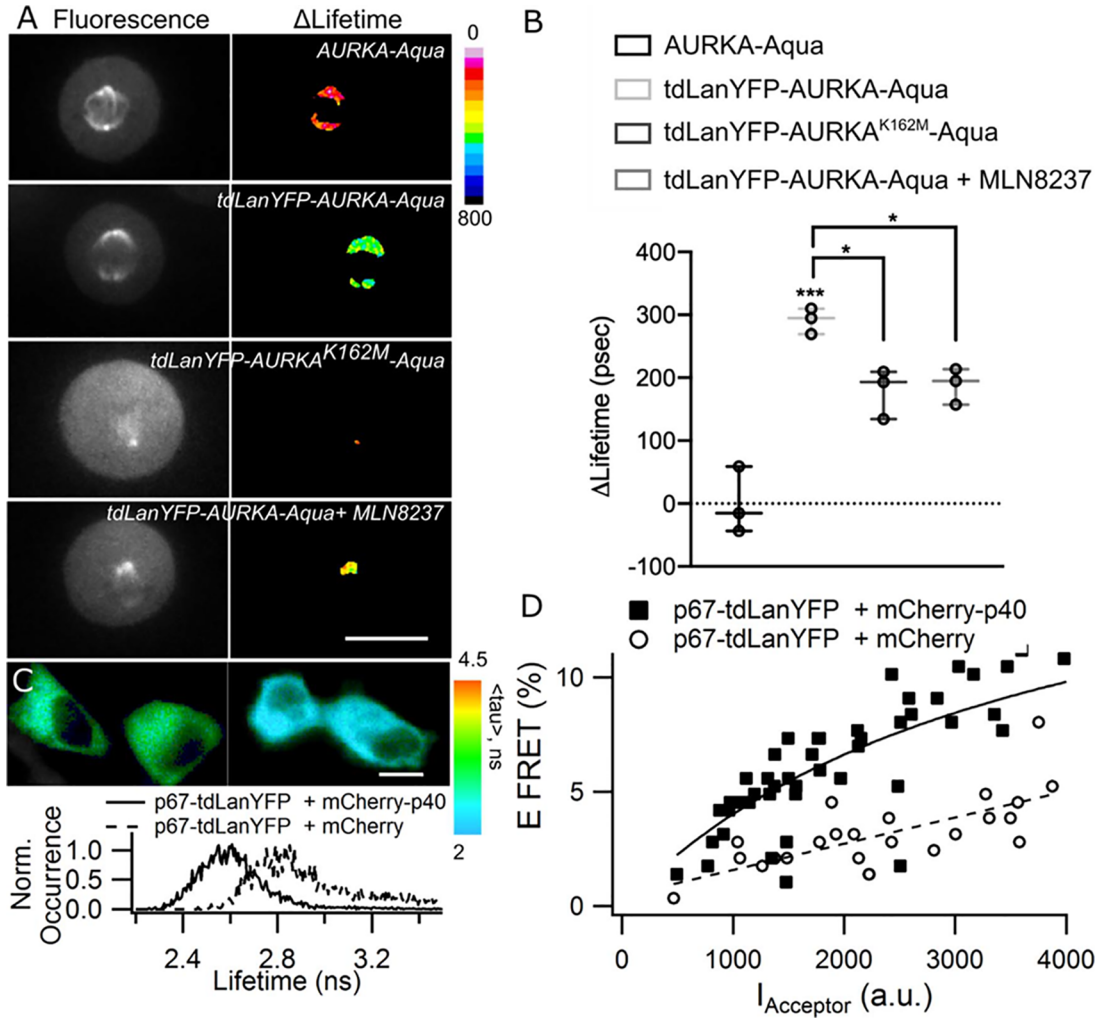

Figure 5. (A) Representative fluorescence intensity (Aquamarine channel) and ΔLifetime images of U2OS cells expressing the indicated constructs and synchronized at mitosis (scale bar, 10 μm), together with (B) the corresponding ΔLifetime quantification at the mitotic spindle. The bar in boxplots represents the median; whiskers extend from the 10th to 90th percentiles. Circles represent the mean FRET values issued by three independent experiments, where 10 cells per experiment were analyzed. (C) Representative FLIM images of COS7 cells expressing p67-tdLanYFP with mCherry (left) or mCherry-p40 (right) and the corresponding lifetime histograms. Scale bar, 10 μm. (D) Average FRET efficiencies plotted against the acceptor (mCherry) fluorescence intensity. Each symbol represents the values for one cell. Solid and dashed lines are for eye guidance only.

Applications of tdLanYFP as a FRET Partner for Live-Cell Imaging. To validate further the Aquamarine/tdLanYFP as a FRET pair, we built a biosensor reporting the autophosphorylation of protein kinase AURKA and tdLanYFP-AURKA-Aquamarine, as well as a kinase-dead version, the mutant AURKA(K162M), as a control (Figure 5A, B).[27] We evaluated their responses by FRET/FLIM on the mitotic spindle in U2OS cells synchronized at mitosis. Aquamarine-AURKA served as a lifetime reference. In the case of the AURKA kinase-responsive biosensor version, we observed a lifetime variation of ∼300 ps corresponding to the FRET from Aquamarine to tdLanYFP upon autophosphorylation. This was a variation slightly higher than the value observed recently with the mTurquoise2/tdLanYFP FRET pair.[27] We also observed that the kinase-dead version did not completely abolish FRET, neither did the ATP analog MLN8237 used to inhibit AURKA autophosphorylation,. This was consistent with previous observations done for the biosensor built with the mTurquoise2/tdLanYFP pair.[27] As a rule of thumb, an efficient energy transfer can be observed up to twice R_0, the Förster distance. For Aquamarine/tdLanYFP and mTurquoise2/tdLanYFP FRET pairs, R_0 values are around ∼60 Å. For the AURKA kinase-responsive and kinase-dead version of the biosensor, the donor−acceptor distances were estimated as 83 and 97 Å, respectively.[27] These two values are below twice R_0 (∼120 Å), and therefore, FRET may be observed even within the more elongated inhibited or kinase-dead versions of the biosensor.

We also evaluated the possibility to use tdLanYFP as a FRET donor in intermolecular FRET. As a model, we used two subunits of the NADPH oxidase, p67^{phox} and p40^{phox}, that are known to interact in the resting state of the enzyme.[3] The subunits were transiently expressed in COS7 cells, and FRET was monitored by TCSPC-FLIM (Figure 5C, D). As a reference, we monitored the lifetime of p67-tdLanYFP coexpressed with mCherry. We observed a significant decrease in the donor lifetime when the two protein partners, p67-tdLanYFP and mCherry-p40, were coexpressed (Figure 5C). For each cell, the FRET efficiency was plotted against $I_{Acceptor}$ (Figure 5D). Interestingly, we noticed a nonspecific FRET

https://doi.org/10.1021/acssensors.1c00874
ACS Sens. 2021, 6, 3940−3947

likely due to crowding that started even at the lowest analyzed fluorescence intensities of the acceptor, whether the FRET acceptor mCherry is fused to the $p40^{phox}$ subunit or not (Figure 5D). However, the FRET efficiency for the coexpression of p67-tdLanYFP with mCherry-p40 was always above the control, reaching a value of around 10% for the highest fluorescence intensities of the acceptor, consistent with our previous observations with the same proteins of interest and Citrine as a donor.[3] It is thus possible to exchange Citrine for tdLanYFP in such experiments.

The use of a dimer as an acceptor may have various consequences on the efficiency of the FRET phenomenon. To follow protein−protein interaction, a more bulky dimer may impair the interaction and appear as a drawback. Nevertheless, the dimer is composed of two potential acceptors with different orientations, which may be beneficial for the energy transfer. Thus, the FRET efficiency, induced by the protein−protein interaction, might be less orientation-dependent. For FRET-based biosensors, the benefit may depend on the nature of the conformational change induced by the sensing central module located between the donor and the acceptor. If the conformational change induces a large distance effect between completely close and open conformations for example, the use of a dimer may be useful to limit orientational effects. On the contrary, if the FRET variation in the biosensor is mostly related to an orientational effect itself between an orientation with minimal FRET in one conformation and an orientation with maximal FRET in the other, a large FRET variation might be harder to achieve with a dimer. Indeed each monomer could be a potential efficient acceptor in both conformations.

Finaly, here, we report a lifetime-based FRET detection for the biosensors. For ratiometric detection of FRET on a dedicated microscopy setup, the blue-shifted fluorescence emission spectrum of tdLanYFP in comparison to classical YFPs may necessitate the use of a narrower band-pass emission filter for the detection channel of the donor alone. As a result, this may slightly decrease the signal-to-noise ratio in such ratiometric detection.

CONCLUSIONS

In this work, we show that tdLanYFP is a high-performance yellow fluorescent protein for monitoring intracellular biological processes in various biosensing modalities, which can be used as a classic label or in FRET-based strategies. Its characteristics surpass those of the currently available yellow fluorescent proteins derived from the original EYFP.

In vitro, dLanYFP keeps most of the oustanding properties of the wild-type LanYFP, which are the best features for a yellow fluorescent protein including brightness per chain that is 1.7 times higher than that of Citrine and a fluorescence lifetime of 2.9 ns. The tandem dimeric version tdLanYFP retains the same photophysical characteristics as dLanYFP. Constructed for live-cell experiments, it allows most of the conventional imaging applications using the spectral selection available for conventional YFPs. Its photostability is a great advantage for applications requiring high-power illumination or long-time observations of a small pool of proteins, for example, single-molecule tracking or analysis of kinetics even in super-resolved imaging as STED microscopy. Its low $pK_{1/2}$ allows monitoring of FRET at pH as low as 6 without any variation of FRET efficiency. These properties pave the way for new applications in acidic environements including the development of biosensors for the acidic degradative compartments of the endocytic and autophagic pathways or for the phagosomes, acidic traps of immune cells to destroy microbes. Those machineries are involved in many physiopathological processes, and molecular tools such as genetically encoded biosensors are still missing mainly due to the lack of FPs that are able to be a reliable optical reporter at acidic pH values.[12,28] tdLanYFP was successfuly integrated in a FRET-based biosensor in conjunction with a cyan donor. In most cases, the structural rationale behind a FRET biosensor, *i.e.*, the range of conformations probed by the FRET pair involving a whole set of possible distances and orientations, is not known and requires a trial-and-error approach. In this report, we presented tdLanYFP that will be a valuable probe for any experiment requiring a photostable acceptor with low pH sensitivity.

Even though the tandem can now be used as it is in FRET-based applications, its relatively slow maturation and residual oligomerization tendency could remain a drawback in particular for quantitative hetero-FRET applications. The maturation may be further improved by several rounds of mutagenesis. Nevertheless, the screening for fast-maturating versions of tdLanYFP should be performed while preserving the incredible brightness, excellent photostability, and low pH sensitivity of the current version of the protein.

EXPERIMENTAL PART

Details on molecular biology and *in vitro* experiments can be found in the Supporting Information.

Live-Cell Experiments. Most of the live-cell experiments were performed in COS7. Cells were cultivated in DMEM Glutamax (Invitrogen) supplemented with 5% FCS in 25 cm^2 flasks. For microscopy, cells were grown to 80% confluence on a glass coverslip (ibidi) and transiently transfected with the appropriate expression plasmids with XtremeGene HP (Roche Diagnostics) following the supplier's instructions and used 24−48 h after the transfection.[3] An AURKA FRET biosensor was expressed in U2OS cells. The cells were cultivated, transfected, and synchronized at mitosis as previously described.[27]

Microscopy. *Wide-Field Bleaching Experiments.* Wide-field bleaching experiments were performed either on purified 6xHis-tagged fluorescent proteins attached to Ni-NTA agarose beads or on COS7 cells expressing cytosolic constructs. In both cases, the epifluorescence pathway of the TCSPC-FLIM setup (see below) was used for illumination, and fluorescence was excited and collected through a Semrock Brightline cube YFP-2427B-NTE-ZERO. The incident power on the sample was 530 μW, and the diameter of the illumination field was 400 μm, giving an approximate irradiance of 0.4 W/cm^2. Averages of 5 to 10 individual intensity decay traces were collected for each sample type and fitted with single- or double-exponential decay models as required, from which the average bleaching time was computed.

OSER Assay. For OSER assay, COS7 cells expressing the OSER construct of either tdLanYFP or Citrine targeted to the endoplasmic reticulum were imaged with an inverted Leica DMI8 microscope equipped with a 40×/0.6 NA objective (Leica) and piloted with Metamorph software. The epifluorescence pathway was equipped with a solid-state light engine (Lumencor), a set of filter cubes, and a CCD camera (Flash4.0LT, Hamamatsu Photonics). We used the Semrock Brightline cube YFP-2427B-NTE-ZERO for spectral selection. Images were analyzed visually using ImageJ. Typical examples of OSER cases are shown in Figure S9 for tdLanYFP (750 cells classified) and Citrine (420 cells classified).

Confocal Images. Confocal images were acquired with an inverted Leica DMI 6000 microscope equipped with a 63×/1.4 NA PL APO oil immersion objective (Leica) and piloted with LAS-X software (Leica). Excitation was performed at 510 nm with a white light laser, and the fluorescence was detected between 525 and 570 nm with a GaAsP Hybride detector (Hamamatsu).

https://doi.org/10.1021/acssensors.1c00874
ACS Sens. 2021, 6, 3940−3947

Photobleaching in Confocal Conditions and STED Imaging. For the photobleaching in confocal conditions and for STED imaging, LifeAct-mCitrine and LifeAct-tdLanYFP expressed in COS7 cells were imaged with an inverted Leica TCS SP8 gated-STED super-resolution microscope (Leica) equipped with a 100×/1.40 NA HCX PL APO STED oil immersion objective and piloted with Leica SP8 LAS AF software (version 3.6; Leica). The instrument was equipped with a WLL Laser (511 nm excitation wavelength) and a 592 nm depletion laser. The depletion laser was operated at an average power of 70% of 400 mW with a gated detection of T_g = 1.5−6 ns. The variations of the fluorescence intensities within the cells during the time lapse over 30 frames in confocal imaging were measured in several ROIs in the cells and averaged. The final data are the average of three different cells.

FCS Experiments. For FCS experiments, an inverted Leica confocal microscope TCS SP8 SMD (Leica) was used. It was equipped with a DMI 6000 CS stand and a 63×/1.2 NA HC PLAN APO water immersion objective. The samples were excited with a continuous argon laser at 514 nm, and the fluorescence was selected by a 505 nm dichroic mirror and a band-pass filter of BP 540/30 nm with an APD detector (PicoQuant). For the detection, the SMD module was constituted of a PicoHarp 3000 system for TTTR mode of single-photon counting (PicoQuant). The fluctuations of fluorescence intensity were autocorrelated, and the resulting curves were analyzed using a standard pure diffusion model with SymphoTime (PicoQuant).

Fast-FLIM. Fast-FLIM measurements were performed on a Leica DMI6000 microscope (Leica) equipped 63×/1.4 NA oil immersion objective and a time-gated custom-built setup for FLIM[29] and driven by Inscoper hardware (Inscoper). Briefly, cells were excited at 440 ± 10 nm using a white light pulsed laser (Fianium), and emission was selected using a band-pass filter of 483/35 nm. The detection was time-gated, and the fluorescence lifetime was calculated with five sequential temporal gates of 2.2 ns each. The mean pixel-by-pixel lifetime was calculated only when the fluorescence intensity was above 3000 gray values using Inscoper software (Inscoper). To calculate the ΔLifetime, the mean lifetime of the cells expressing the donor alone (AURKA-Aquamarine) was calculated, and its value was used to normalize data in all the analyzed conditions for each experiment.

TCSPC-FLIM Microscopy. TCSPC-FLIM microscopy was performed using a custom-made time-resolved laser scanning TCSPC microscope described previously.[7] Briefly, the setup is based on a TE2000 microscope with a 60×, 1.2NA water immersion objective (Nikon). The epifluorescence pathway was equipped with a solid-state light engine (Lumencor), a set of filter cubes, and a CCD camera (ORCA AG, Hamamatsu Photonics). The spectral selections for CFP, YFP, and RFP are available Table S1. The CFP cube was used for Aquamarine, the YFP cube was used for EYFP, Citrine, dLanYFP, and tdLanYFP, and the RFP cube was used for mCherry. A spectrometer (Ocean Optics) was fixed on the front exit of the microscope with an optical fiber. The emission spectra were recorded with the CFP excitation filter on the whole field of view (Figure S11). The TCSPC path was equipped with 440 and 466 nm pulsed laser diodes (PicoQuant) driven by a PDL800 driver (20 MHz, PicoQuant) for CFP and YFP, respectively. The fluorescence was selected by a set of filters (Table S2) with an MCP-PMT detector (Hamamatsu Photonics). The C1 scanning head (Nikon) probed a 100 μm × 100μm field of view. The PicoHarp300 TCSPC module (PicoQuant) collected all the signals, and data were processed with SymPho-Time64 software (PicoQuant). The TCSPC fluorescence decay of all the pixels of the cytosol was computed by the SymPhoTime64, and decays were fitted with exponential fit functions:

$$I(t) = \text{background} + I_0 \times \sum_i \alpha_i e^{-(t/\tau_i)}$$

The quality of the fit was evaluated by the weighted residual distribution and Pearson's χ^2 test. The average lifetime was computed as $\langle\tau\rangle = \sum_i \alpha_i\tau_i$, and the apparent FRET efficiency was calculated using $\langle\tau_{DA}\rangle$, the average lifetime of the donor in the presence of an acceptor, and τ_{Donor}, the lifetime of the donor alone:

$$E_{FRET} = 1 - \frac{\langle\tau_{DA}\rangle}{\tau_{Donor}}$$

We observed a slight decrease in the donor lifetime when the fluorescence intensity of the acceptor, $I_{Acceptor}$, in the cell increased (Figure S12). $I_{Acceptor}$ is directly proportional to the concentration of the tandems in the cell cytosol in the case of Figure S12. When their concentration increased, a heteromolecular FRET between close tandem molecules can happen in addition to the intramolecular one within the tandems, leading to the observed concentration-dependent lifetime decrease.[30] To minimize the effect of the so-called molecular crowding on the intramolecular FRET efficiency, we set a maximum limit for $I_{Acceptor}$ at which the donor lifetime decreased less than 5% ($I_{Acceptor}$ < 1000 a.u.) in the tandem experiment. In Figure 5, the nonspecific FRET due to crowding was directly evaluated by comparing the evolution of FRET efficiencies in the presence of mCherry only with the ones in the presence of mCherry fused to p40, the interaction partner of p67.

■ ASSOCIATED CONTENT

Supporting Information

The Supporting Information is available free of charge at https://pubs.acs.org/doi/10.1021/acssensors.1c00874.

All details for plasmid construction and for *in vitro* expression and characterization of the recombinant proteins as well as supplementary figures and tables (PDF)

■ AUTHOR INFORMATION

Corresponding Author

Marie Erard − *Université Paris-Saclay, CNRS, Institut de Chimie Physique, 91405 Orsay, France;* orcid.org/0000-0002-4063-365X; Phone: +33 1 69 15 30 14; Email: marie.erard@universite-paris-saclay.fr

Authors

Yasmina Bousmah − *Université Paris-Saclay, CNRS, Institut de Chimie Physique, 91405 Orsay, France*

Hana Valenta − *Université Paris-Saclay, CNRS, Institut de Chimie Physique, 91405 Orsay, France*

Giulia Bertolin − *Univ Rennes, CNRS, IGDR (Institut de génétique et développement de Rennes)−UMR 6290, 35000 Rennes, France*

Utkarsh Singh − *Université Paris-Saclay, CNRS, Institut de Chimie Physique, 91405 Orsay, France*

Valérie Nicolas − *Microscopy Facility (MIPSIT), Ingénierie et Plateformes au Service de l'Innovation Thérapeutique−IPSIT−UMS−US31−UMS3679 (IPSIT), Université Paris-Saclay, 92296 Châtenay-Malabry, France*

Hélène Pasquier − *Université Paris-Saclay, CNRS, Institut de Chimie Physique, 91405 Orsay, France*

Marc Tramier − *Univ Rennes, CNRS, IGDR (Institut de génétique et développement de Rennes)−UMR 6290, 35000 Rennes, France;* orcid.org/0000-0001-8200-6446

Fabienne Merola − *Université Paris-Saclay, CNRS, Institut de Chimie Physique, 91405 Orsay, France*

Complete contact information is available at: https://pubs.acs.org/10.1021/acssensors.1c00874

Funding

This work was supported by LabEx PALM Grant ANR-10-LABX-0039-PALM and by the IDEX Paris Saclay (IRS

BioProbe). H.V. was supported by a Ph.D. fellowship from MESRI.

Notes

The authors declare no competing financial interest.

■ ACKNOWLEDGMENTS

This work has benefited from the SpICy microscopy facility of ICP for TSCPC-FLIM measurements, the Microscopy Rennes Imaging Centre (MRic) for FCS and Fast-FLIM measurements, the Plateforme d'Imagerie Cellulaire MIPSIT for STED measurements, and the Light Microcopy Facility Imagerie-Gif for confocal microscopy. We thank P. Pernot for the analysis of the fluorescence decays.

■ REFERENCES

(1) Greenwald, E. C.; Mehta, S.; Zhang, J. Genetically Encoded Fluorescent Biosensors Illuminate the Spatiotemporal Regulation of Signaling Networks. *Chem. Rev.* **2018**, *118*, 11707−11794.
(2) Padilla-Parra, S.; Tramier, M. FRET Microscopy in the Living Cell: Different Approaches, Strengths and Weaknesses. *BioEssays* **2012**, *34*, 369−376.
(3) Ziegler, C. S.; Bouchab, L.; Tramier, M.; Durand, D.; Fieschi, F.; Dupré-Crochet, S.; Mérola, F.; Nüße, O.; Erard, M. Quantitative Live-Cell Imaging and 3D Modeling Reveal Critical Functional Features in the Cytosolic Complex of Phagocyte NADPH Oxidase. *J. Biol. Chem.* **2019**, *294*, 3824−3836.
(4) Zhou, X.; Mehta, S.; Zhang, J. Genetically Encodable Fluorescent and Bioluminescent Biosensors Light Up Signaling Networks. *Trends Biochem. Sci.* **2020**, *45*, 889−905.
(5) Mérola, F.; Fredj, A.; Betolngar, D.-B.; Ziegler, C.; Erard, M.; Pasquier, H. Newly Engineered Cyan Fluorescent Proteins with Enhanced Performances for Live Cell FRET Imaging. *Biotechnol. J.* **2014**, *9*, 180−191.
(6) Tsien, R. Y. The Green Fluorescent Protein. *Annu. Rev. Biochem.* **1998**, *67*, 509−544.
(7) Erard, M.; Fredj, A.; Pasquier, H.; Beltolngar, D.-B.; Bousmah, Y.; Derrien, V.; Vincent, P.; Merola, F. Minimum Set of Mutations Needed to Optimize Cyan Fluorescent Proteins for Live Cell Imaging. *Mol. BioSyst.* **2013**, *9*, 258−267.
(8) Goedhart, J.; van Weeren, L.; Hink, M. A.; Vischer, N. O. E.; Jalink, K.; Gadella, T. W. J., Jr. Bright Cyan Fluorescent Protein Variants Identified by Fluorescence Lifetime Screening. *Nat. Methods* **2010**, *7*, 137−139.
(9) Goedhart, J.; von Stetten, D.; Noirclerc-Savoye, M.; Lelimousin, M.; Joosen, L.; Hink, M. A.; van Weeren, L.; Gadella, T. W. J., Jr.; Royant, A. Structure-Guided Evolution of Cyan Fluorescent Proteins towards a Quantum Yield of 93%. *Nat. Commun.* **2012**, *3*, 751.
(10) Casey, J. R.; Grinstein, S.; Orlowski, J. Sensors and Regulators of Intracellular PH. *Nat. Rev. Mol. Cell Biol.* **2010**, *11*, 50−61.
(11) Poëa-Guyon, S.; Pasquier, H.; Mérola, F.; Morel, N.; Erard, M. The Enhanced Cyan Fluorescent Protein: A Sensitive PH Sensor for Fluorescence Lifetime Imaging. *Anal. Bioanal. Chem.* **2013**, *405*, 3983−3987.
(12) Nault, L.; Bouchab, L.; Dupré-Crochet, S.; Nüße, O.; Erard, M. Environmental Effects on Reactive Oxygen Species Detection—Learning from the Phagosome. *Antioxid. Redox Signaling* **2016**, *25*, 564−576.
(13) Griesbeck, O.; Baird, G. S.; Campbell, R. E.; Zacharias, D. A.; Tsien, R. Y. Reducing the Environmental Sensitivity of Yellow Fluorescent Protein: mechanism and applications. *J. Biol. Chem.* **2001**, *276*, 29188−29194.
(14) Zacharias, D. A. Partitioning of Lipid-Modified Monomeric GFPs into Membrane Microdomains of Live Cells. *Science* **2002**, *296*, 913−916.
(15) Kremers, G.-J.; Goedhart, J.; van Munster, E. B.; Gadella, T. W. J. Cyan and Yellow Super Fluorescent Proteins with Improved Brightness, Protein Folding, and FRET Förster Radius. *Biochemistry* **2006**, *45*, 6570−6580.
(16) Wiens, M. D.; Hoffmann, F.; Chen, Y.; Campbell, R. E. Enhancing Fluorescent Protein Photostability through Robot-Assisted Photobleaching. *Integr. Biol.* **2018**, *10*, 419−428.
(17) Shaner, N. C.; Lambert, G. G.; Chammas, A.; Ni, Y.; Cranfill, P. J.; Baird, M. A.; Sell, B. R.; Allen, J. R.; Day, R. N.; Israelsson, M.; Davidson, M. W.; Wang, J. A Bright Monomeric Green Fluorescent Protein Derived from Branchiostoma Lanceolatum. *Nat. Methods* **2013**, *10*, 407−409.
(18) Cranfill, P. J.; Sell, B. R.; Baird, M. A.; Allen, J. R.; Lavagnino, Z.; de Gruiter, H. M.; Kremers, G.-J.; Davidson, M. W.; Ustione, A.; Piston, D. W. Quantitative Assessment of Fluorescent Proteins. *Nat. Methods* **2016**, *13*, 557−562.
(19) Betolngar, D.-B.; Erard, M.; Pasquier, H.; Bousmah, Y.; Diop-Sy, A.; Guiot, E.; Vincent, P.; Mérola, F. pH Sensitivity of FRET Reporters Based on Cyan and Yellow Fluorescent Proteins. *Anal. Bioanal. Chem.* **2015**, *407*, 4183−4193.
(20) Clavel, D.; Gotthard, G.; von Stetten, D.; De Sanctis, D.; Pasquier, H.; Lambert, G. G.; Shaner, N. C.; Royant, A. Structural Analysis of the Bright Monomeric Yellow-Green Fluorescent Protein MNeonGreen Obtained by Directed Evolution. *Acta Crystallogr., Sect. D: Struct. Biol.* **2016**, *72*, 1298−1307.
(21) Bajar, B.; Wang, E.; Zhang, S.; Lin, M.; Chu, J. A Guide to Fluorescent Protein FRET Pairs. *Sensors* **2016**, *16*, 1488.
(22) Campbell, R. E.; Tour, O.; Palmer, A. E.; Steinbach, P. A.; Baird, G. S.; Zacharias, D. A.; Tsien, R. Y. A Monomeric Red Fluorescent Protein. *Proc. Natl. Acad. Sci. U. S. A.* **2002**, *99*, 7877−7882.
(23) Shaner, N. C.; Campbell, R. E.; Steinbach, P. A.; Giepmans, B. N. G.; Palmer, A. E.; Tsien, R. Y. Improved Monomeric Red, Orange and Yellow Fluorescent Proteins Derived from Discosoma Sp. Red Fluorescent Protein. *Nat. Biotechnol.* **2004**, *22*, 1567−1572.
(24) Costantini, L. M.; Fossati, M.; Francolini, M.; Snapp, E. L. Assessing the Tendency of Fluorescent Proteins to Oligomerize Under Physiologic Conditions. *Traffic* **2012**, *13*, 643−649.
(25) Valenta, H.; Erard, M.; Dupré-Crochet, S.; Nüβe, O. The NADPH Oxidase and the Phagosome. In *Molecular and Cellular Biology of Phagocytosis*; Hallett, M. B., Ed.; Advances in Experimental Medicine and Biology; Springer International Publishing: Cham, 2020; Vol. *1246*, pp. 153−177, DOI: 10.1007/978-3-030-40406-2_9.
(26) Lambert, T. J. FPbase: A Community-Editable Fluorescent Protein Database. *Nat. Methods* **2019**, *16*, 277−278.
(27) Bertolin, G.; Sizaire, F.; Déméautis, C.; Chapuis, C.; Mérola, F.; Erard, M.; Tramier, M. Optimized FRET Pairs and Quantification Approaches To Detect the Activation of Aurora Kinase A at Mitosis. *ACS Sens.* **2019**, *4*, 2018−2027.
(28) Lie, P. P. Y.; Nixon, R. A. Lysosome Trafficking and Signaling in Health and Neurodegenerative Diseases. *Neurobiol. Dis.* **2019**, *122*, 94−105.
(29) Bertolin, G.; Sizaire, F.; Herbomel, G.; Reboutier, D.; Prigent, C.; Tramier, M. A FRET Biosensor Reveals Spatiotemporal Activation and Functions of Aurora Kinase A in Living Cells. *Nat. Commun.* **2016**, *7*, 12674.
(30) Grailhe, R.; Merola, F.; Ridard, J.; Couvignou, S.; Le Poupon, C.; Changeux, J.-P.; Laguitton-Pasquier, H. Monitoring Protein Interactions in the Living Cell Through the Fluorescence Decays of the Cyan Fluorescent Protein. *Eur. J. Chem. Phys.* **2006**, *7*, 1442−1454.